J Fluoresc (2017) 27:199–203
DOI 10.1007/s10895-016-1946-5

ORIGINAL ARTICLE

Structural and Near-Infrared Properties of Nd^{3+} Activated Lu_3NbO_7 Phosphor

Mustafa İlhan[1] · **Mete Kaan Ekmekçi**[2] · **Rıza Gürcan Oraltay**[3] · **Ali Sadi Başak**[2]

Received: 13 July 2016 / Accepted: 3 October 2016 / Published online: 28 October 2016
© Springer Science+Business Media New York 2016

Abstract Undoped and Nd^{3+} doped lutetium niobate phases have been prepared by a conventional solid state reaction method using lutetium acetate and niobium oxide at 1250 °C for 6 h. X-ray diffraction patterns of the 6 mol% Lu_3NbO_7 sample exhibited a cubic fluorite single phase. Phase structure exhibited interesting crystallization behaviour depending on increasing Nd^{3+} concentration which led to a Lu_3NbO_7 single phase formation during the heat treatment process. SEM investigations were also in agreement with the XRD results. Morphologies of Nd^{3+} doped lutetium niobate powders exhibited oval like shapes and grain sizes varied between 0.3 and 5 μm. Near-infrared luminescence properties of Nd^{3+} doped Lu_3NbO_7 were also studied. 1.06 μm laser transition characteristics of Nd^{3+} doped lutetium niobate have been observed. Concentration quenching phenomenon was not detected depending on increasing Nd^{3+} doping concentrations at room temperature.

Keywords Ln_3NbO_7 · Niobates · Phosphors · Solid state synthesis · Neodymium doping

✉ Mustafa İlhan
mustafa.ilhan@marmara.edu.tr

[1] Department of Metallurgical and Materials Engineering, Marmara University, Göztepe Kampüsü, Kadıköy, 34722 İstanbul, Turkey

[2] Department of Chemistry, Marmara University, Göztepe Kampüsü, Kadıköy, 34722 İstanbul, Turkey

[3] Department of Environmental Engineering, Marmara University, Göztepe Kampüsü, Kadıköy, 34722 İstanbul, Turkey

Introduction

Owing to the increasing need of energy storage, lighting, display and laser application technologies, environmentally harmless, highly luminous and low cost multifunctional materials have attracted great attention as the alternative to existing technologies over the past decades [1, 2]. Luminescence properties of the various phosphor materials highly depend on the crystal structures of the host lattice and the nature of the activator ion. Thus, choosing the proper host lattice and the activator ion plays a key role in phosphor synthesis and their potential usage in technological area [3–5]. In order to fabricate functional crystals as optical materials, doping of rare earth ions have been performed intensively [6, 7]. Among the rare earths, Nd^{3+} has been extensively used as a laser active ion in different hosts and lasers [8–10]. Among many rare earth active ions, Nd^{3+} has efficient lasing properties due to its multiple absorption levels in UV, visible, and NIR spectral regions. Nd^{3+} doped fibers are used as tunable laser material in telecommunication field. Various host materials doped with Nd^{3+} have been used at 1060 and 1350 nm for laser applications [11, 12].

Niobates and tantalates have played important role in different technological fields. Cubic fluorite-type rare-earth niobates, RE_3NbO_7, have attracted great attention due to their electro-optical, photocatalytic, magnetic and dielectric properties [13–18]. In recent years, electrical and magnetic properties of Ln_3MO_7 compounds such as: (M = Mo, Ru, Ir, Os, and Re were intensively investigated [19–26]. Moreover, the structural and dielectric properties of Ln_3NbO_7 (Ln = Nd, Gd, Dy, Er, Lu Yb and Y) ceramics were also studied [27]. The Ho_3NbO_7 shows an antiferromagnetic transition at 1 K, while Dy_3NbO_7 and Gd_3NbO_7 are paramagnetic [28]. The photocatalytic activities of RE_3TaO_7 and RE_3NbO_7 (RE) rare earths Y, Yb, Gd, or La) have been investigated previously

[29]. Lu_3NbO_7 has used as micro lens and scintillators due to its high refractive index and high density [30].

The Ln_3NbO_7 (Ln = Nd, Gd, Dy, Er, Lu Yb and Y) type niobates show different crystal systems. For example, Sm_3NbO_7 and Gd_3NbO_7 have weberite-type orthorhombic structure, while cubic defect fluorite-type or pyrochlore-type structure has been reported for Ln_3NbO_7 compounds [27]. The fluorite structure (AO_2) is capable to construct superstructures with its flexible nature [31]. The Ln_3NbO_7 structure shows different polymorph properties depending on the ionic radius. Ln ions having larger ionic radius show cation-ordering [17, 18] and smaller ions exhibit a cation-disordering [18, 27, 31]. So, rare-earth cations with small ionic radii (RE = Y, Dy, Ho, Er, Tm, Yb and Lu), have a cubic defect-fluorite structure (Fm3m). In this structure, RE and Nb cations randomly occupy the 4a site in the rate of 3 to 1, and 1/8 of the 8c site for O anion respectively. [31]. So, oxygen defects and cation disordering make this host material interesting for dopant ions. Up to this time, investigations have been mostly focused on the preparation of Lu_3NbO_7 powders [26, 30], crystal structure refinement [26] and transparency of polycrystalline or single crystal Lu_3NbO_7 [32]. However, except the study on Eu^{3+} doped Lu_3NbO_7 [33], there are still lack of investigations on the optical properties of such materials doped with rare earth ions. To our knowledge, no study has been conducted on the near infrared luminescence properties of Nd^{3+} doped cubic fluorite-type Lu_3NbO_7. Here, we have reported the synthesis, interesting crystallization behaviour, microstructural and optical characterizations of undoped and Nd^{3+} doped cubic fluorite-type Lu_3NbO_7 phosphors.

Experimental

Undoped and Nd^{3+}doped lutetium niobate ($0.5 \leq x \leq 6$ mol%) ceramic powders were synthesized by a solid state reaction method. Lutetium acetate tri hydrate ($Lu(CH_3COO)_3.3H_2O$) with purity of 99 % (Sigma-Aldrich) and Nb_2O_5 with purity of 99.9 % (Alfa Aesar) powders were used as starting materials. Nd_2O_3 with purity of 99.9 % (Alfa Aesar) was used as a dopant. $Lu(CH_3COO)_3.3H_2O$ and Nb_2O_5 powder mixtures were prepared according to Ln_3NbO_7 stoichiometry. The undoped and Nd_2O_3 doped powder mixtures were homogenized in agate mortar. Afterwards, the powder mixture was placed in an alumina crucible and then calcined at 1250 °C temperature for 6 h.

The phase compositions and crystallography parameters for sintered samples were determined by X-ray diffractometer (XRD, Rigaku Corp., D-MAX 2200) using Cu-K_α radiation at a scan rate of 2°/min between 20 and 65° and Ni filter. The crystallography parameters of Ln_3NbO_7 compound were calculated by using MDI Jade 6.5 program. The morphology and elemental composition of the sintered powders were investigated by Scanning electron microscopy (SEM, JEOL Ltd., JSM-5910LV) equipped with Energy dispersive spectroscopy (EDS, OXFORD Industries INCAx-Sight 7274; 133-eV resolution 5.9 keV) after Au/Pd (gold/palladium) coating. Emission spectra of the powders doped with Nd^{3+} ions were measured in the wavelength-range of 850–1450 nm, under 800 nm excitation from a diode laser (LDI-820). Fluorescence from the samples were focused on the slit of a Monochromator (Mc Pearson Model 2051) and detected by PMT (Hamamatsu 7102) detector. All of the photoluminescence measurements were performed at room temperature.

Results and Discussion

X-Ray Diffraction and SEM-EDS Analyses

Figure 1 shows the XRD patterns of the main Lu_3NbO_7 (JCPDS Card No. 24–1089) and minor $LuNbO_4$ (JCPDS Card No. 23–1207) phases. XRD analysis revealed that, a single Lu_3NbO_7 structure occurred for 6 mol% Nd^{3+} doped powders, while $LuNbO_4$ minor phase was detected for undoped, 0.5 and 3 mol% Nd^{3+} doped powders respectively. In literature, Lu_3NbO_7 single phase structure was obtained by using from 1200 to 1650 °C calcination temperatures under high atmospheric pressures [32, 33]. Here, Lu_3NbO_7 structure exhibited interesting crystallization behaviour by increasing of Nd^{3+} doping concentration which led to a single phase formation during the heat treatment process. Such phenomenon can be attributed to the enhancement of rare earth ions on the liquid phase formation, diffusion process and crystallization ability of the structure [34]. When our synthesis temperature (1250 °C) compared to literature temperature, increasing of Nd^{3+} concentration could be lead to the single phase

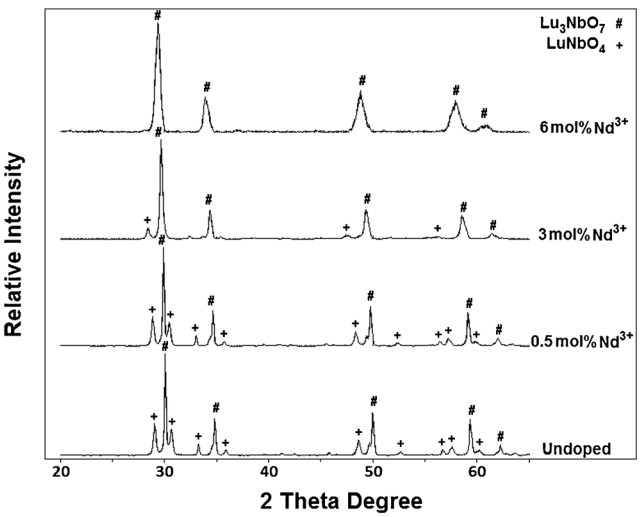

Fig. 1 XRD patterns of undoped and 0.5, 3 and 6 mol% Nd^{3+} doped powders

Table 1 Crystallography and lattice parameters

Crystallography data		
Formula	Lu_3NbO_7	
Crystal system	Cubic fluorite	[35]
Space group	*Fm3m (225)*	[35]
$a = b = c$ (Å)	5.1979	[35]
V(Å^3)	140.44	[35]
Z	-	
2θ range (deg.)	20–65	
Step (deg./min.)	2	
Program	MDI Jade 6.5	
Lattice data		
Nd^{3+} concentration (%)	$a = b = c$ (Å)	V (Å^3)
0.5	5.5957 (4)	175.21
3	5.8458 (4)	199.77
6	6.1418 (4)	231.68

formation similar as pressure effect which has been reported in the above mentioned literature.

XRD analysis indicated that 6 mol% Nd^{3+} doped powder with single phase crystallized in cubic fluorite symmetry with space group: *Fm3m* (*225*). It was also reported by An et al. [35] that, Lu_3NbO_7 has a cubic fluorite structure with cell parameters of a = 5.1979 Å, b = 5.1979, c = 5.1979 Å and V = 140.44 (Å)^3. Lattice parameters of 0.5, 3 and 6 mol% Nd^{3+} doped powders were presented in Table 1. As it is seen from the Table 1 that, lattice constant of the doped powders increased by increasing Nd^{3+} doping concentration and varied from 5.5957 Å to 6.1418 Å for doping levels of 0.5 and 6 mol% respectively. The onset of diffraction peaks with increasing intensity indicated a shift to smaller angles showing the expansion of the lattice due to ionic size effect ($r_{cation}/r_{anion} \approx 0.69$ and C.N. of Nd^{+3} is 6) [36]. Because of the attractive ionic forces between anions and cations, lattice expanded up to 6 mol% Nd^{3+} doping concentration. Consequently, neodymium ions could have easily occupied the vacant sites of lattice leading a single phase formation, which depends on the enhancement of diffusion process and crystallization behaviour.

SEM investigations were also in agreement with the XRD results. Figure 2a–d shows the SEM micrographs of undoped and 0.5, 3 and 6 mol% Nd^{3+} doped samples. SEM analysis revealed that the grain size of Lu_3NbO_7 remarkably decreased for doped samples with the increasing concentrations of Nd^{3+} ions up to 6 mol%. Morphologies of Nd^{3+} doped Lu_3NbO_7 powders exhibited oval like shapes and grain sizes varied between 0.3 and 5 μm. SEM and EDS analyses also revealed differences in the elemental compositions between Lu_3NbO_7, and $LuNbO_4$ grains. EDS analyses was performed at 10 kV of SEM acceleration voltage in order to detect the smaller grains present at surface. SEM micrograph and EDS spectrums of 3 mol% Nd^{3+} doped sample were given in Fig. 3a–c. In EDS analyses, atomic ratio of Lu/Nb was found to be about 3:1 for Lu_3NbO_7 grains (point 1 in Fig. 3b). As it can be seen from the (point 2 in Fig. 3c), Lu/Nb ratio decreased for grains of $LuNbO_4$ that formed mostly between Lu_3NbO_7 grains. As seen from the XRD results, $LuNbO_4$ phase disappeared for

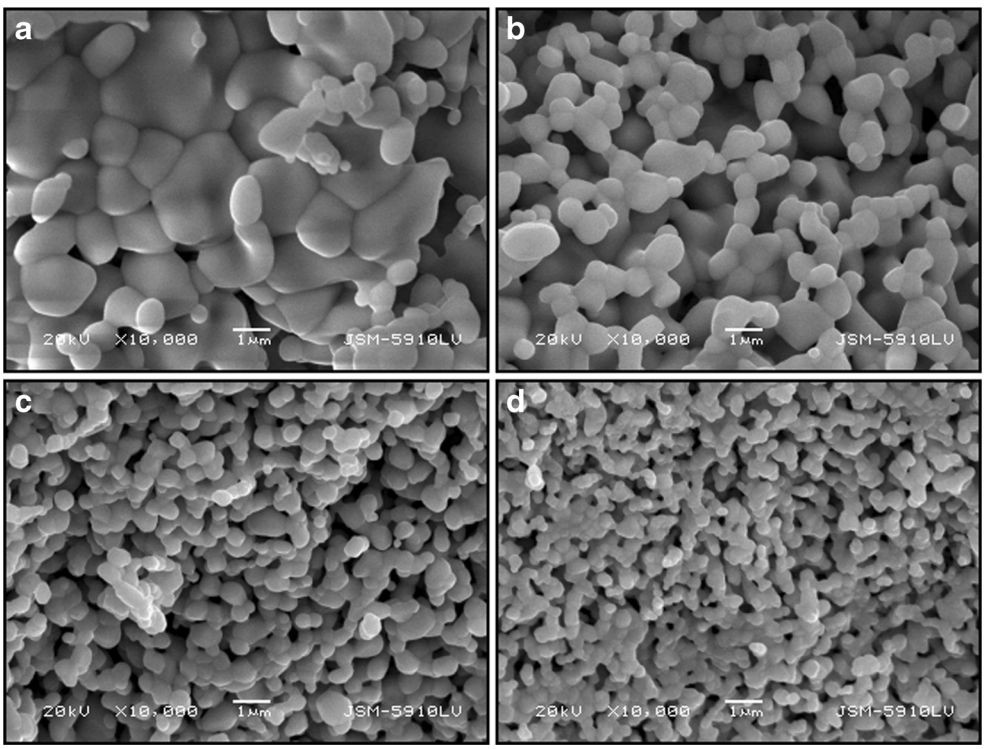

Fig. 2 SEM micrographs of undoped and 0.5, 3 and 6 mol% Nd^{3+} doped powders

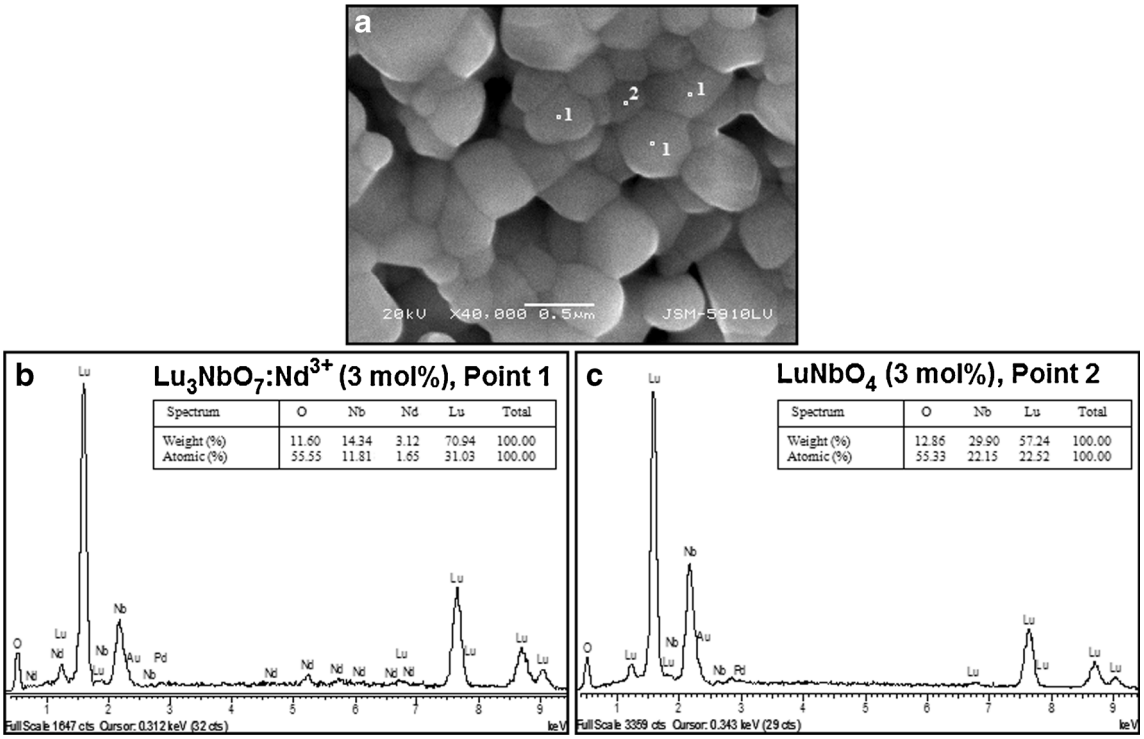

Fig. 3 SEM and EDS analyses of 3 mol% doped Nd^{3+} sample; SEM seconder electron (SE) micrograph at 40.000× magnification (**a**), EDS spectra of Lu_3NbO_7:Nd^{3+}grains (point 1) (**b**), and $LuNbO_4$ grains (point 2) (**c**)

6 mol% Nd^{3+} doped sample. XRD and SEM-EDS results also claimed that, incorporation of Nd^{3+} ions may affect the charge compensation which promoted the single phase formation in the structure.

Optical Analyses

Absorption spectrum of Lu_3NbO_7 host lattice are given in Fig. 4. Corresponding to spectrum, energy gap for electron transition between the valence and the conduction bands was calculated in the range of 3.71-3.77 eV. Also, the excitation band centered at 296 nm [33] is attributed to the charge-transfer (CT) transitions by the electron transfer from filled 2p orbital of O^{2-} ions to vacant 4f orbital of Eu^{3+} ion.

The emission spectra of Lu_3NbO_7:Nd^{3+} powders were measured in the 850–1450 nm range, under 800 nm excitation. Three characteristic bands were observed corresponding to the transitions from the $^4F_{3/2}$ to $^4I_{11/2}$ and $^4I_{9/2}$ levels. Emission spectra of the laser transition at 1062 nm due to $^4F_{3/2} \rightarrow {}^4I_{11/2}$ transition measured at 300 K are shown in Fig. 5. Although XRD analysis did not show any minor peak for 6 mol% Nd^{3+} doped sample, a small peak appeared at 1100 nm which may possibly due to presence of $LuNbO_4$

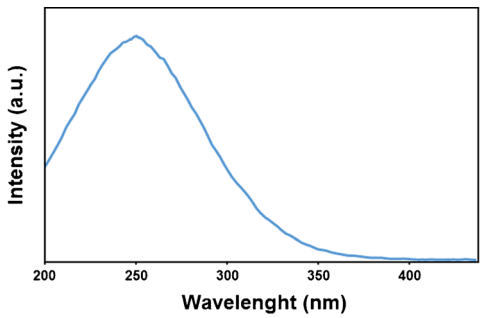

Fig. 4 Absorption spectrum of Lu_3NbO_7 host lattice

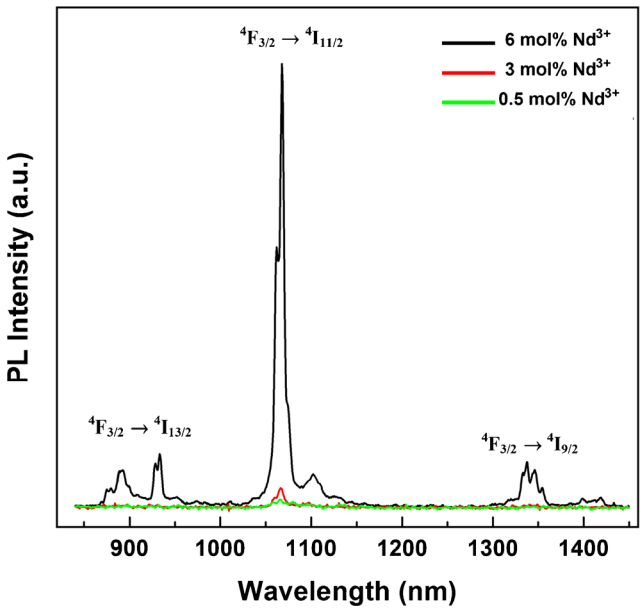

Fig. 5 Emission spectra of lutetium niobate powders for the $^4F_{3/2} \rightarrow {}^4I_{13/2}$, $^4I_{11/2}$, $^4I_{9/2}$ transitions

phase. The assignments of the different emission bands were identified on the basis of Dieke's energy level diagram [37]. As it can be seen from the emission spectra, J-manifolds of Nd^{3+} ions were split due to symmetry of Lu_3NbO_7 cation sites. The spectral profile and the number of the Stark components were same for 0.5, 3 and 6 mol% Nd^{3+} doped powder. This behaviour can be explained by the local symmetry of ligands surrounding of Nd^{3+} ions. Increasing of local symmetry of ligands in Lu_3NbO_7 phase may have dependently increased the emission intensity. Consequently, increased near-infrared photon intensity may attributed to structural changes, loss of $LuNbO_4$ phase and increase of Lu_3NbO_7 phase whereas 6 mol% Nd^{3+} doped phosphor exhibited the highest emission intensity.

Conclusion

Undoped and Nd^{3+} doped lutetium niobate crystalline powders were synthesized by solid state synthesis method annealed at 1250 °C for 6 h. XRD analysis revealed a single phase for 6 mol% Nd^{3+} doped powders with cubic fluorite structure, while $LuNbO_4$ minor phase was detected for 0.5 and 3 mol% Nd^{3+} doped powders. Lu_3NbO_7 structure exhibited interesting crystallization behaviour by increasing of doping concentration which led to a single phase formation. When our synthesis temperature (1250 °C) compared to literature temperature, increasing of Nd^{3+} concentration could be lead to the single phase formation similar as pressure effect. SEM-EDS analyses revealed a decrease in grain size depending on increasing Nd^{3+} doping concentration. The near-infrared emission intensity of niobate crystalline powders increased with increasing dopant concentration up to 6 mol%.

References

1. Başak AS, Ekmekçi MK, Erdem M, İlhan M, Mergen A (2016) J Fluoresc 26:719–724
2. Ekmekçi MK, İlhan M, Başak AS, Deniz S (2015) J Fluoresc 25: 1757–1762
3. Vishwnath V, Srinivas M, Patel NP, Modi D, Murthy KVR (2016) J Fluoresc 26:277–282
4. Devi HJ, Singh WR, Loitongbam RS (2016) J Fluoresc 26:875–889
5. Giri NK, Mishra K, Rai SB (2011) J Fluoresc 21:1951–1958
6. Ferriol M (2001) Prog Cryst Growth Charact Mater 43:221–244
7. Torres ME, Kaminskii AA, Silgo CG, Plat JG, Jaque D, Rodenas A, Martin IR, Lavin V (2008) J Alloy Compd 451:198–200
8. Chaliha RS, Annapurna K, Tarafder A, Tiwari VS, Gupta PK, Karmakar B (2010) Opt Mater 32:1202–1209
9. Dawar AL, Mehta V, Mansingh A, Rup R (1997) OptMater 7:33–39
10. Daqin C, Yuansheng W, Yunlong Y, Feng L, Ping H (2008) J Rare Earths 26:428–431
11. Mahmoud KH (2014) Opt Commun 320:68–72
12. Choi JH, Margaryan A, Margaryan A, Shi FG (2005) J Lumin 114: 167–177
13. Yang H, Liu X, Zhou Z, Guo L (2013) Catal Commun 31:71–75
14. İlhan M, Ekmekçi MK (2015) J Solid State Chem 226:243–249
15. Abe R, Higashi M, Sayama K, Abe Y, Sugihara H (2006) J Phys Chem B 110:2219–2226
16. Subramanian MA, Aravamudan G, Rao GVS (1983) Prog Solid State Chem 15:55–143
17. Rooksby HP, White EAD (1964) J Am Ceram Soc 47:94–96
18. Garton G, Wanklyn BM (1968) J Mater Sci 3:395–401
19. Greedan JE, Raju NP, Wegner A, Gougeon P, Padiou J (1997) J Solid State Chem 129:320–327
20. Nishimine H, Wakeshima M, Hinatsu Y (2005) J Solid State Chem 178:1221–1229
21. Van Berkel FPF, Ijdo DJW (1986) Mater Res Bull 21:1103–1106
22. Harada D, Hinatsu Y (2002) J Solid State Chem 164:163–168
23. Nishimine H, Doi Y, Hinatsu Y, Sato M (2007) J Ceram Soc Jpn 115:577–581
24. Plaisier JR, Drost RJ, Ijdo DJW (2002) J Solid State Chem 169: 189–198
25. Lam R, Langet T, Greedan JE (2003) J Solid State Chem 171:317–323
26. Doi Y, Harada Y, Hinatsu Y (2009) J Solid State Chem 182:709–715
27. Cai L, Nino JC (2007) J Eur Ceram Soc 27:3971–3976
28. Cashion JD, Cooke AH, Leask MJM, Thorp TL, Wells MR (1968) J Mater Sci 3:402–407
29. Abe R, Higashi M, Zou Z, Sayama K, Abe Y, Arakawa H (2004) J Phys Chem B 108:811–814
30. Leitner J, Chuchvalec P, Sedmidubsky D, Strejc A, Abrman P (2003) Thermochim Acta 395:27–46
31. Klimenko AN, Kozlov YS, Sergeev VS, Pastukhov EA (1992) Thermochim Acta 209:331–338
32. An L, Ito A, Goto T (2011) Mater Lett 65:3167–3169
33. Du Y, Zhang Y, Huang K, Wang S, Yuan L, Feng S (2013) Dalton Trans 42:8041
34. Wang J, Liu ZW, Zheng ZG, Yu HY, Tang GP, Zeng DC (2015) Mater Lett 159:76–79
35. An L, Iton A, Goto T (2013) Ceram Int 39:383–387
36. Speight JG (1999) Lange's handbook of chemistry Sixteenth Edition. The McGraw-Hill Companies, New York
37. Dieke GH (1968) Spectra and energy levels of rare earth ions in crystals, Interscience Publishers, New York